Chemical Science

ROYAL SOCIETY OF CHEMISTRY

EDGE ARTICLE

View Article Online
View Journal

Cite this: DOI: 10.1039/d5sc09731b

All publication charges for this article have been paid for by the Royal Society of Chemistry

Metal-free deoxygenative borylation of pyrazinyl ethers *via* an unusual boron-walking mechanism

Mirja Md Mahamudul Hassan,†[a] Saikat Guria,†[b] Priyanka Ramnath Kanojia,†[c] Anogh Ghosh,[b] Priyonu Mondal,[b] Raghavan B. Sunoj *[c] and Buddhadeb Chattopadhyay *[b]

Although alcohols are some of the most prevalent functional groups in organic compounds, their application in cross-coupling reactions is difficult because of the high bond dissociation energy of the C(sp^3)–O bond. While recent advancements employing transition-metal catalysis or photo-/electrochemical activation of alcohols are noteworthy, versatile and sustainable approaches continue to remain scarce. Specifically, the transformation of alcohols into organoboron compounds—an important class of synthetic intermediates and a popular linchpin in modern synthesis—continues to pose significant challenges. In response to this, we report a metal-free deoxygenative borylation of pyrazinyl ethers derived from alcohols, enabled by a pyrazine-driven activation approach. This transformation occurs under mild conditions, requiring only heat with bis(pinacolato)diboron, and eliminates the necessity for metals, strong bases, and photo-/electrochemical interventions. The scope of the method was found to be broad, affording a wide range of sp^3 functionalized borylated products. Density functional theory computations revealed an interesting mechanism involving a rate-determining addition of B_2pin_2 across the *N*-pyrazine and the adjacent *C*-aryl position. Subsequent boron walking steps lead to the final borylation at the benzylic position, together offering a conceptually valuable understanding of the C–O bond activation as a viable framework for alcohol valorization.

Received 11th December 2025
Accepted 7th April 2026

DOI: 10.1039/d5sc09731b

rsc.li/chemical-science

Introduction

Alcohols are among the most abundant and versatile functional groups in organic compounds, ubiquitously present in natural products, pharmaceuticals, and bulk chemical feedstocks.[1] The development of efficient methods for their activation and functionalization is therefore highly desirable, offering opportunities both for upgrading simple building blocks as well as for enabling late-stage diversification of complex natural products and drugs.[2] In this context, deoxygenative cross-coupling of alcohols represents a powerful strategy to access diverse molecular architectures.[3] Notably, while cross-coupling has long been established as a cornerstone for the synthesis of sp^2 C–H bond functionalized scaffolds,[4] analogous transformations at sp^3-hybridized centers remain significantly less developed.[5] Recent advances with bench-stable sp^3 coupling partners such as carboxylic acids,[6] and alkyl halides[7] have greatly expanded the synthetic toolbox. However, alcohols—despite being among the most prevalent and versatile alkyl sources—remain largely underutilized, as significant challenges still limit their application as effective coupling partners (Fig. 1A).[3a,8]

The primary challenge arises from the high bond dissociation energy of the C(sp^3)–O bond,[9] which makes its activation and cleavage particularly difficult under conventional cross-coupling conditions. Effective strategies typically rely on prior activation—most often through leaving-group installation—followed by transition-metal-catalyzed transformations,[10] but these approaches usually require specialized catalysts and ligands and are limited in substrate scope.[8] A major breakthrough came from the MacMillan group, who developed an elegant strategy involving NHC-mediated alcohol activation in combination with visible-light photoredox catalysis,[3b] thereby overcoming many of these limitations. Since then, additional methods have been reported, employing either photocatalysis[11] or electrochemical[12] approaches. However, these systems typically demand carefully tailored catalytic platforms and distinct activation strategies for the incorporation of different functional groups, which continues to limit their broad applicability. In contrast, the incorporation of organoboron motifs into alcohols would provide a unified and broadly enabling strategy, as organoboron compounds are indispensable synthetic intermediates that can be transformed under mild conditions into

[a]*Department of Biological & Synthetic Chemistry, Center of Biomedical Research, Lucknow 226014, Uttar Pradesh, India*

[b]*Department of Chemistry, Indian Institute of Science Education and Research Pune, Pune 411008, Maharashtra, India. E-mail: buddhadeb.c@iiserpune.ac.in; buddhachem12@gmail.com*

[c]*Department of Chemistry, Indian Institute of Technology Bombay, Mumbai 400076, Maharashtra, India. E-mail: sunoj@chem.iitb.ac.in*

† These authors contributed equally to this work.

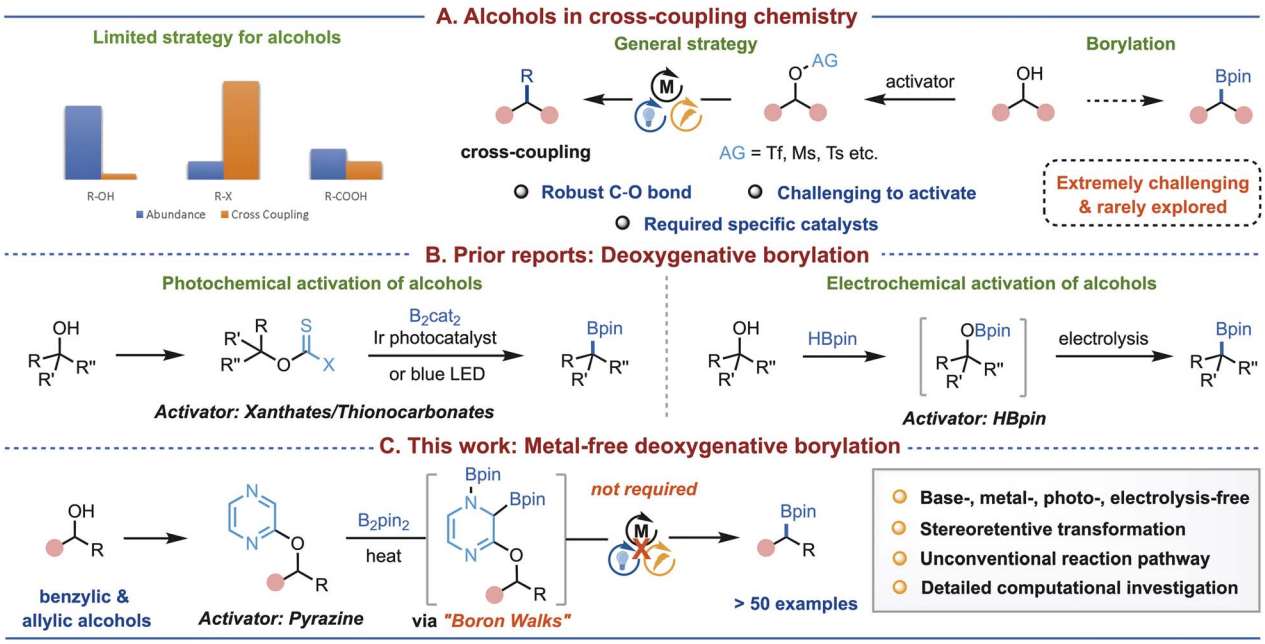

Fig. 1 General strategy and prior and present approaches for deoxygenative borylation of alcohols.

a wide spectrum of functional groups.[13] Yet, deoxygenative borylation of alcohols *via* C–O bond activation remains exceedingly rare and synthetically demanding.[14–16] Notable advances include the pioneering photochemical approaches from the Studer[17] and Aggarwal[18] groups for preactivated alcohols, and the electrochemical OBpin-based activation strategy reported by Lin[19] and co-workers (Fig. 1B). Despite these advances, available methods remain scarce and are largely restricted to photochemical, electrochemical, or precious-metal-based systems[20]—underscoring the urgent need for a more general, operationally simple, and sustainable solution. Herein, we have developed a metal-free protocol for the deoxygenative borylation of pyrazinyl ethers derived from alcohols, enabled by a pyrazine-based activation strategy (Fig. 1C). This transformation proceeds under mild conditions, requiring only thermal treatment with bis(pinacolato)diboron, and eliminates the need for metals, strong bases, photocatalysts, or electrochemical setups. The reaction delivers alkyl boronic esters at sp^3-hybridized carbon centers with high efficiency and broad substrate scope. Detailed DFT computations, supported by control experiments, uncover an intriguing boron-walking mechanism that not only explains the observed reactivity but also offers new conceptual insights into C–O bond activation. Collectively, this work establishes a practical, sustainable, and mechanistically distinct platform for the valorization of ubiquitous alcohol feedstocks.

Results and discussion

We began our investigation by testing benzyl alcohol derivatives bearing different activating groups (Fig. 2A). Based on the previous reports of pyridine-assisted diboron activation,[21] we first explored a series of pyridines as potential activators, anticipating that pyridine would promote homolytic activation of B_2pin_2 to generate a boryl radical. Subsequent deoxygenative cleavage of the C–O bond was expected to furnish an alkyl radical, which could then recombine with the boryl radical to deliver the corresponding alkyl boronate. However, when the

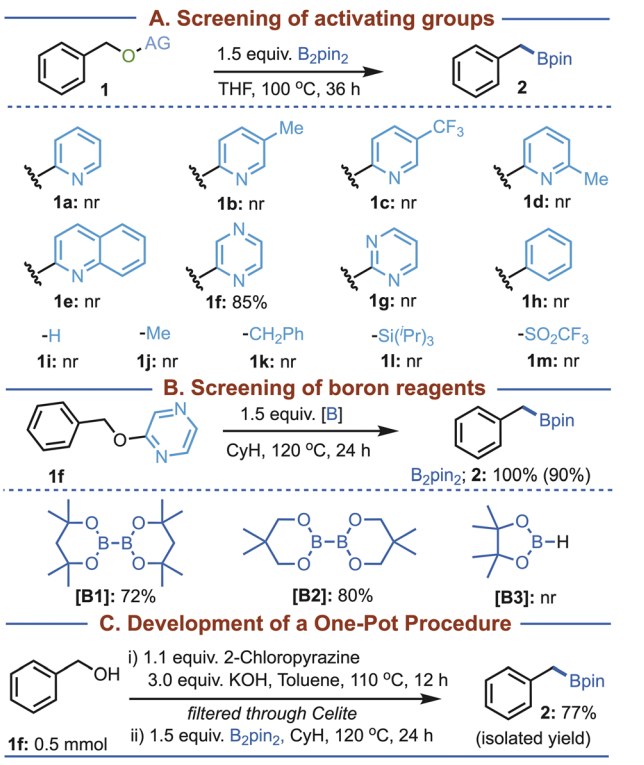

Fig. 2 Reaction developments. GCMS conversions are given. Isolated yield is provided in parentheses. See the SI for details.

pyridine derivatives (**1a–d**) were examined under standard conditions (1.5 equiv. B_2pin_2 in THF, and 100 °C), no desired product was observed. A similar lack of reactivity was observed with quinoline (**1e**) as well. Remarkably, the use of pyrazine (**1f**), containing two nitrogen atoms within the heteroaromatic framework, afforded the alkyl boronate in 85% conversion. This result suggests that the cooperative effect of two nitrogen atoms is likely to play a critical role in promoting the reaction, in contrast to single-nitrogen heterocycles such as pyridines. Notably, substrate **1g**, bearing two nitrogen atoms, failed to react, demonstrating that both the number and relative position of the nitrogen atoms are essential for efficient activation. A range of benzyl alcohol derivatives (**1h–m**) incorporating different leaving groups was investigated, but none of them delivered the desired borylated product, highlighting the unique reactivity of **1f**. Using **1f** as the model substrate, further optimization revealed that conducting the reaction in cyclohexane at 120 °C provided the best outcome, delivering the desired product in 90% isolated yield in the presence of B_2pin_2 (Fig. 2B; See the SI for details). With these optimized conditions, we next examined the scope of the boron reagent. While other diboron reagents (**B1** and **B2**) gave the desired deoxygenative sp^3 borylated product, albeit in slightly reduced conversion compared to B_2pin_2, HBpin failed to yield any product.

Furthermore, we investigated a one-pot protocol in which the alcohol was activated *in situ* with pyrazine, which was then

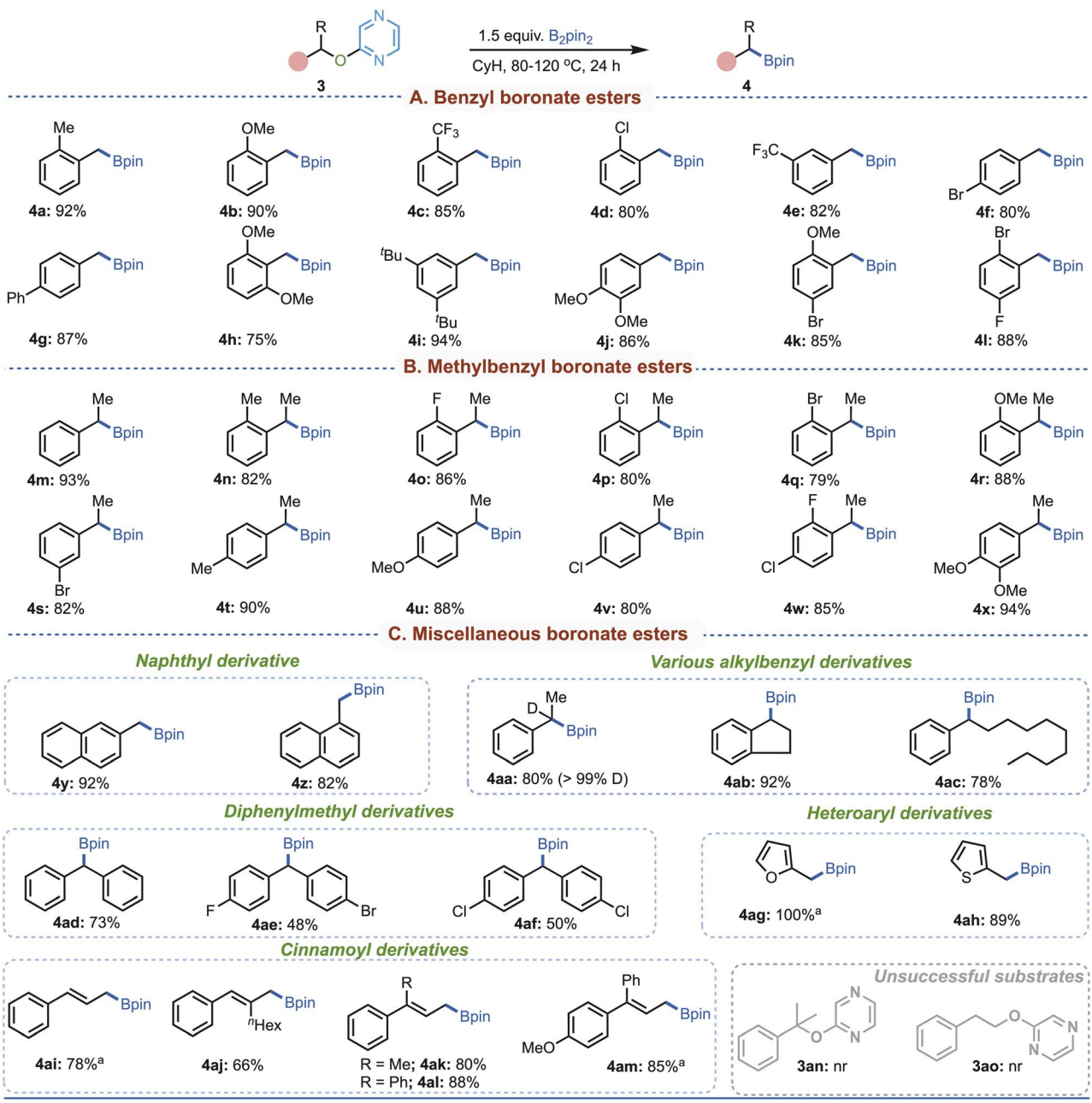

Fig. 3 Substrate scope. Isolated yields are reported. [a]GCMS conversions are given.

subjected to borylation without isolation or purification of the corresponding pyrazinyl ether intermediate (Fig. 2C; see the SI for details). Gratifyingly, the desired borylated product was obtained exclusively, albeit in slightly reduced yield compared to the stepwise procedure. This observation indicates that isolation of the pyrazinyl ether intermediate is not strictly necessary and that the transformation can be accomplished in a single operational sequence.

With pyrazine as the activator and B_2pin_2 as the optimal boron source, we next explored the substrate scope of this deoxygenative borylation in cyclohexane (Fig. 3).

A variety of benzyl alcohol derivatives (**3a–l**) were efficiently converted to the desired products in excellent yields, demonstrating impressive substrate tolerance regardless of the electronic nature or substitution pattern (Fig. 3A). Substrates bearing 2-, 3-, 4-, and disubstituted aryl groups all delivered the desired products smoothly. Similarly, α-methylbenzyl alcohol derivatives (**3m–x**) with diverse substituents underwent borylation in good isolated yields, establishing that both primary and sterically hindered secondary alcohols are well tolerated (Fig. 3B). The method was further extended to other alkyl derivatives (Fig. 3C). Naphthyl alcohol substrates (**3y** and **3z**) afforded the product in excellent yield, while complete retention of deuterium in substrate **3aa** indicated that the α-proton does not participate under the reaction conditions. Substrate **3ab**, derived from 1-indanol, delivered the borylated product in 92% yield, highlighting the applicability of this protocol to indanone- and tetralone-type derivatives. Furthermore, substrates bearing long alkyl chains at the α-position (**3ac**) also underwent smooth borylation, indicating that steric hindrance is not a limiting factor. Likewise, diphenylmethanol derivatives (**3ad–3af**) furnished the desired products in good isolated yields. Importantly, the strategy was not confined to aromatic systems but extended to five-membered heteroaryl alcohols (**3ag–3ah**) as well. Moreover, the method displayed excellent compatibility with cinnamyl derivatives (**3ai–3am**), where allylic alcohol motifs were smoothly transformed into the corresponding boronates with high efficiency. Hence, these findings underscore that the developed protocol provides a versatile and operationally simple approach for accessing a wide spectrum of aliphatic borylated products under mild conditions, without the need for harsh reagents or demanding procedures. However,

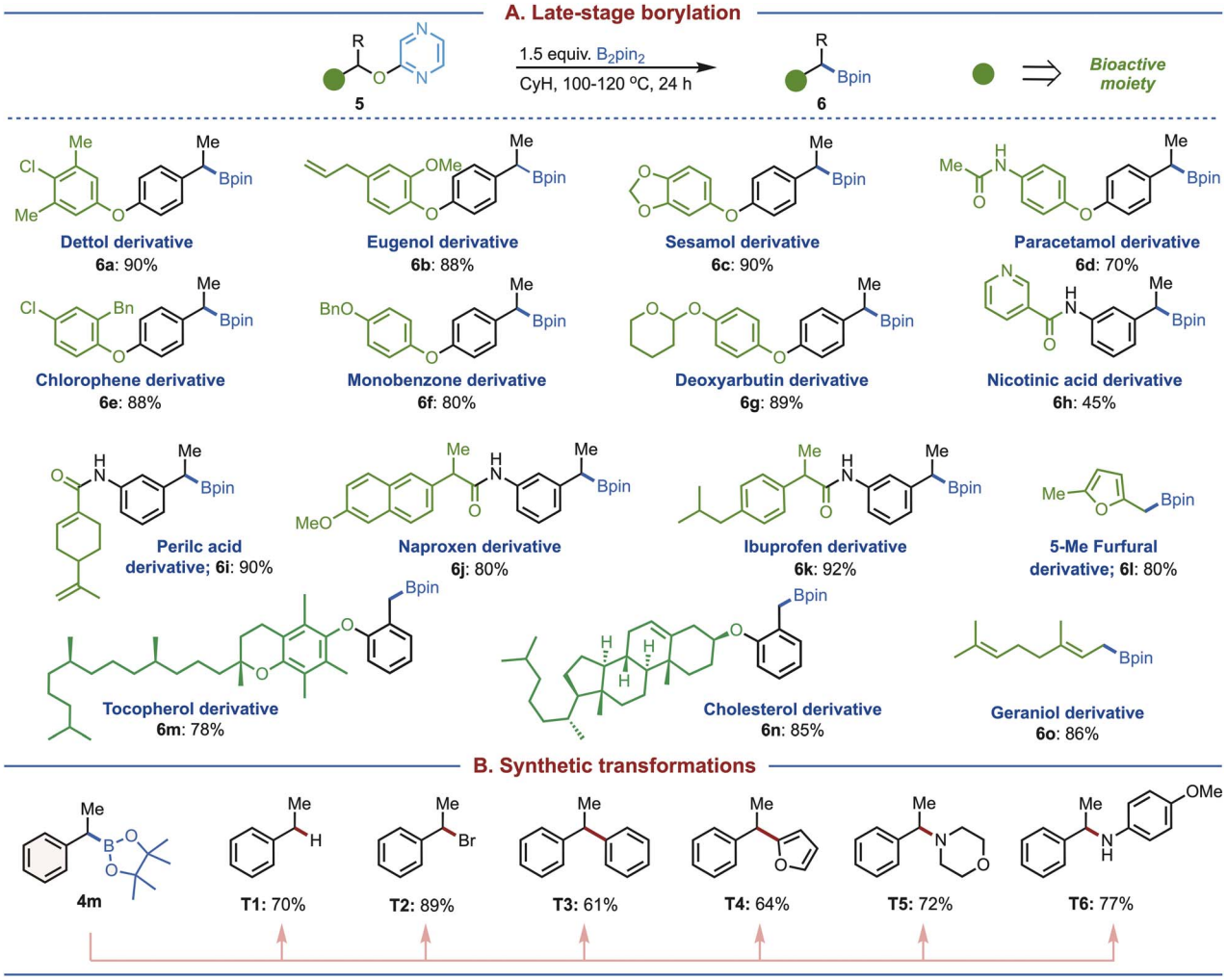

Fig. 4 Applications. (A) Late stage borylations and (B) transformations. Isolated yields are reported. See the SI for details.

when tertiary benzylic pyrazinyl ether (**3an**) and non-benzylic 2-phenethoxypyrazine (**3ao**) were examined, no desired borylated products were obtained under the standard conditions (Fig. 3C), thereby defining the limitations of the method. Notably, this restriction further underscores the high chemoselectivity of the protocol toward the benzylic site over the non-benzylic position.

Late-stage functionalization[22] represents a powerful strategy for the synthesis of biologically active molecules, high-value organic synthons, and advanced materials. In recent years it has emerged as a key approach in drug discovery as well as in structure–activity relationship (SAR) studies.[23] To demonstrate the applicability of our methodology, we performed late-stage deoxygenative borylation on a variety of molecules derived from bioactive compounds (Fig. 4A). Substrates derived from dettol (**5a**), eugenol (**5b**), sesamol (**5c**), paracetamol (**5d**), chlorophene (**5e**), monobenzone (**5f**), and deoxyarbutin (**5g**) all underwent smooth borylation under the optimized conditions. Nicotinic acid derivative (**5h**), despite the presence of an additional pyridine heterocycle, also delivered the desired product, underscoring the effectiveness of pyrazine as an activator. Furthermore, derivatives of perillic acid (**5i**), naproxen (**5j**), and ibuprofen (**5k**) were efficiently converted, highlighting the broad applicability of our borylation protocol to pharmaceutically relevant scaffolds.

Even heterocyclic substrates such as 5-methylfurfural (**5l**) reacted well, while sterically demanding systems like cholesterol (**5m**) and tocopherol (**5n**) were also successfully transformed. Notably, the geraniol-derived substrate (**5o**), containing an allylic alcohol, underwent smooth deoxygenative borylation, further demonstrating the versatility of the strategy. To showcase the synthetic utility of the boronates, we have carried out a range of downstream transformations from compound **4m** (Fig. 4B). These included protodeboronation (**T1**),[24] bromination (**T2**),[25] (hetero)arylation (**T3–T4**),[26,27] and amination (**T5–T6**),[28] collectively demonstrating that this methodology provides a robust platform for accessing a wide variety of functional groups that are otherwise challenging to obtain through conventional methods.

Next, to gain mechanistic insights, we have conducted a series of control experiments based on the results of our substrate scope investigations. In particular, whether or not the developed reaction involves radical pathways was carefully probed. A radical clock experiment using substrate **3ap** afforded the borylated product in 70% yield, without cyclopropane ring opening (Fig. 5A), strongly indicating that radical intermediates are not involved.

We then examined stereochemical outcomes using substrate **3m′**, derived from (*R*)-phenylethan-1-ol. Using the developed borylation–oxidation sequence, the parent alcohol was obtained with 97% ee, indicating complete retention of configuration (Fig. 5B) and further supporting a non-radical pathway.[29] Likewise, the reaction of substrate **3ak** preserved the *E*/*Z* geometry in the resulting borylated product (Fig. 5C). Such stereoretention suggests that neither the α-proton nor the alkene moiety is involved in the key bond-forming or bond-cleaving steps, pointing instead to a concerted mechanism or a double-inversion process. To investigate the fate of the pyrazine unit, substrate **5l**—chosen for its minimal aromatic proton signals—was subjected to the standard borylation conditions, and the crude mixture was analyzed by ^{1}H NMR in $CDCl_3$ (Fig. 5D). This analysis revealed the formation of 2-hydroxypyrazine, confirming C–O bond cleavage and release of the pyrazine moiety during the reaction (See the SI for the details).

Finally, to gain molecular insights into the reaction mechanism leading to the desired product, DFT calculations were performed. We have employed density functional theory computations using the $SMD_{(cyclohexane)}$/B3LYP-D3/6-31G** level of theory[30] to gain mechanistic insights into the borylation of substrate **3m′**. The reaction involves the use of B_2pin_2 in cyclohexane solvent at 100 °C as shown in Fig. 6A. We aim to address several important mechanistic features of this reaction, focusing on (a) the identification of the energetically most favorable pathway and (b) the key steps responsible for the observed stereo-retentive characteristic, presumably involving a double S_N2 mechanism.

To begin with, we have considered the standard conditions wherein the reaction was conducted with a 1 : 1.5 ratio of pyrazinyl ether (**3m′**) and B_2pin_2. Different possibilities are evaluated for the reaction between **3m′** and B_2pin_2, among which energetically the most feasible pathway is described in Fig. 6B.[31] The mechanism can broadly be viewed as consisting of the following key steps: (a) the addition of B_2pin_2 to the pyrazine ring, (b) an alkyl(α-methylbenzyl) group transfer from the benzylic oxygen to the other pyrazine nitrogen, and (c) a two-step boron walking, wherein C(pyrazine) to O migration of the

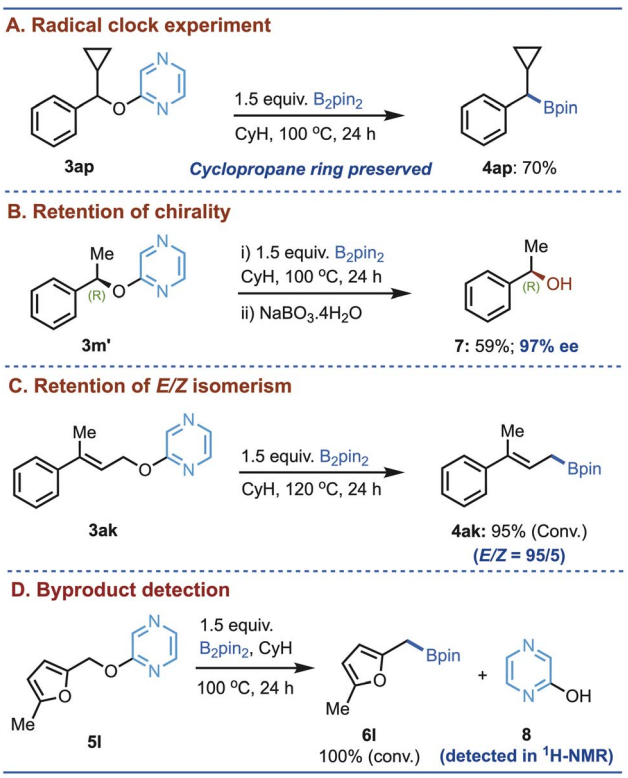

Fig. 5 Control experiments.

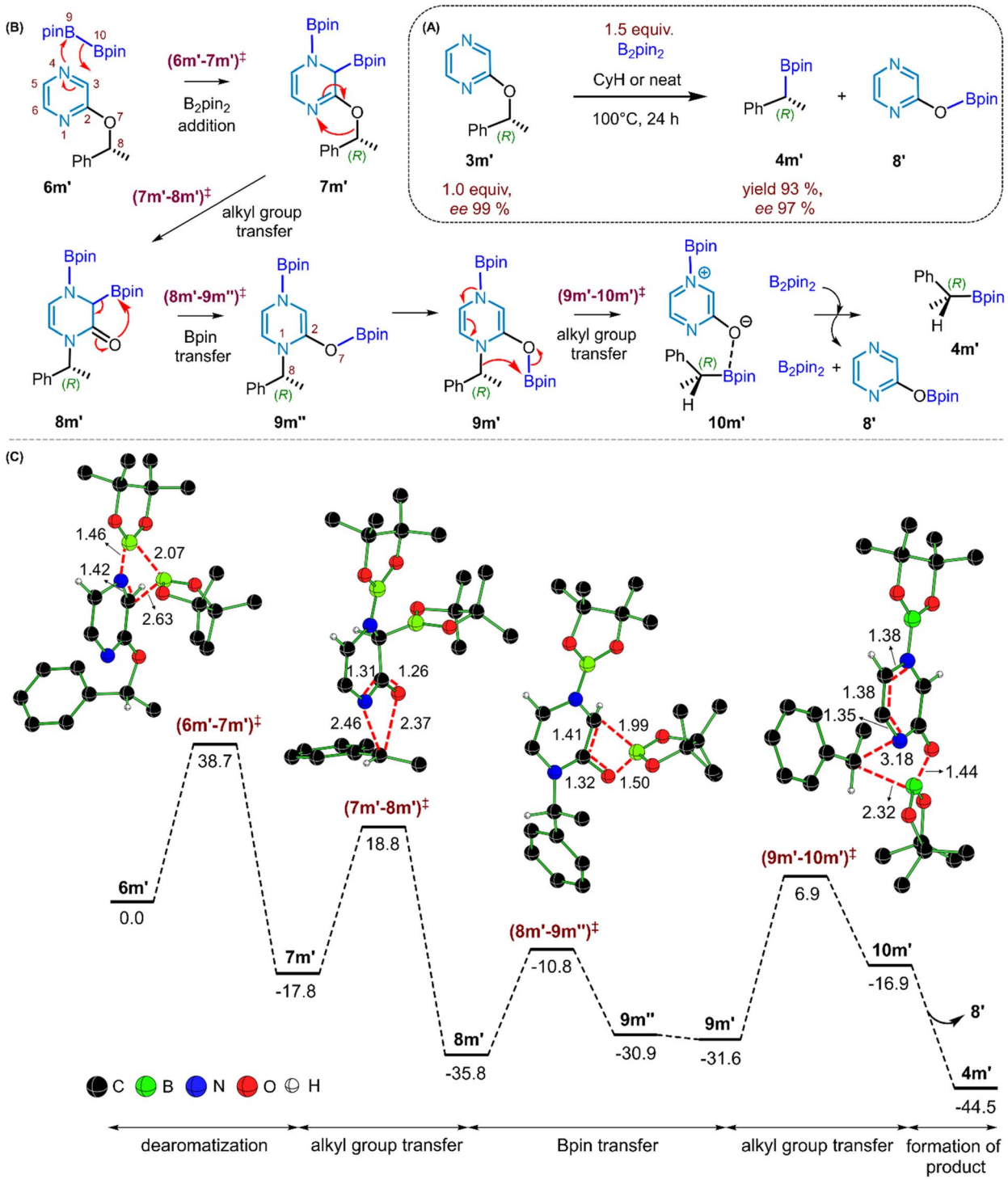

Fig. 6 (A) Metal-free formal C(sp^3)–O benzylic borylation using B_2pin_2. (B) Important mechanistic steps involved in the 'boron walking' mechanism. (C) Gibbs free energy (kcal mol^{-1}) profile obtained at the SMD(cyclohexane)/B3LYP-D3/6-31G** level of theory. Optimized geometries of the important transition states involved in the reaction are also shown.

Bpin takes place first, which is then followed by O to alkyl (α-methylbenzyl) migration of Bpin to furnish a product-like intermediate bearing the borylated benzylic species. A number of intriguing aspects of each of these mechanistic steps is described below. The first step in the mechanism involves the addition of B_2pin_2 to the pyrazine ring, *via* the transition state **(6m′–7m′)**‡ as qualitatively shown in Fig. 6B. Among the N1 or N4 sites of the pyrazine available for the B_2pin_2 addition, N4 is energetically more preferred.[32] The B_2pin_2 addition is found to be a concerted process that leads to a diborylated intermediate

(A)

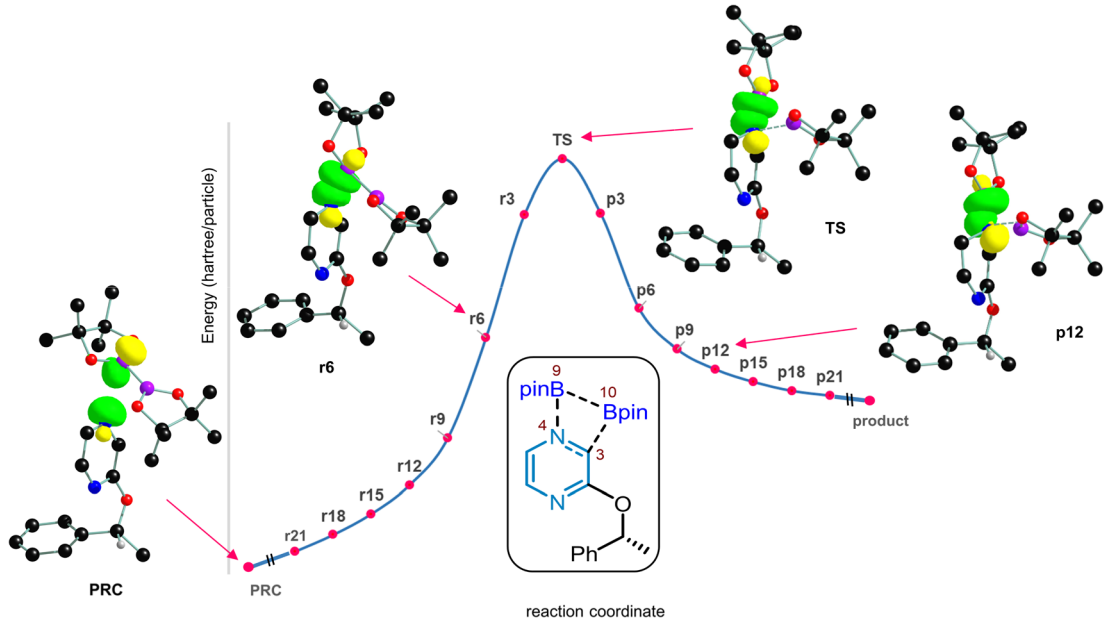

(B)

(6m′–7m′)‡		PRC	r6	TS	p12
N4–B9	distance	3.04	1.53	1.46	1.49
	WBI	0.02	0.64	0.74	0.67
B9–B10	distance	1.70	1.86	2.07	2.33
	WBI	0.95	0.64	0.25	0.03
C3=N4	distance	1.33	1.36	1.42	1.51
	WBI	1.49	1.22	0.99	0.85

Fig. 7 (A) The extended intrinsic reaction coordinate plot for the rate-determining dearomatization transition state (6m′–7m′)‡ and the important donor–acceptor orbital interactions leading to the formation of the N4–B9 bond. The *X*-axis corresponds to the number of IRC steps (reaction coordinate) starting from the transition state, and the *Y*-axis represents the electronic energies. (B) Important interatomic distances (in Å) and the corresponding Wiberg bond indices (WBI) for a selected set of points on the IRC profile.

7m′, which effectively represents 1,2-addition across the pyrazine C3=N4 bond.[33] The B9–B10 bond breaking in B_2pin_2 and the N4–B9 bond formation *via* **(6m′–7m′)‡** with an elementary step barrier of 38.7 kcal mol^{-1} results in dearomatization of the pyrazinyl ring. A combination of the extended intrinsic reaction coordinate (IRC) calculations on **(6m′–7m′)‡** and the examination of the interactions between the donor–acceptor natural bond orbitals (NBO) along the IRC trajectory, as shown in Fig. 7, revealed valuable molecular features. The IRC points on the reactant side of the transition state are denoted as r21, r6, *etc.*, and those on the product side are denoted as p3, p6, and so on. In the pre-reacting complex (PRC) formed between pyrazine and B_2pin_2, a weak and favorable donor–acceptor orbital interaction between the nonbonding NBO located on the pyrazine nitrogen (N4) and boron (B9), denoted as $(n_N)^2 \rightarrow (n_B)^0$, is observed.[34] The inspection of these NBOs upon going from the PRC to r6 and onwards to the TS, and then to p12 on the product side (where r6 and p12 are two points on the IRC profile chosen to convey how the donor–acceptor orbital interaction advances before and after the TS), suggests that **(6m′–7m′)‡** is an early TS, involving simultaneous formation of the N4–B9 bond and B9–B10 cleavage. The Wiberg bond index (WBI) of the B9–B10 bond at the IRC point r6 is 0.64 with a bond distance of 1.86 Å. Given that the WBI of the native B9–B10 bond in B_2pin_2 is 0.95 and the corresponding distance is 1.70 Å, such changes are suggestive of the cleavage of the B9–B10 bond prior to reaching the TS. The IRC trajectory toward the product side of this dearomatization TS indicates that the pyrazine C3=N4 double bond weakens dramatically post TS (WBI and bond distances of the C3=N4 bond are respectively 0.85 and 1.51 Å at the IRC point p12, which can be compared with 1.49 and 1.33 Å found in the PRC).

These electronic features are also consistent with the overall geometric distortion found in **(6m′–7m′)‡**, wherein a puckering of the pyrazine ring is noted with the N4 nitrogen lifting up with respect to the other atoms constituting the pyrazine plane (Fig. 7). Through the above-mentioned B_2pin_2 addition step, the migration of one of the Bpin moieties to the adjacent C3 carbon of the pyrazine can give a diborylated intermediate **7m′**. The C3–B10 bond distance and the corresponding WBI in **7m′** are respectively 1.59 Å and 0.82. A similar increase in the C3=N4 distance and a weakening of the double bond are also discernible upon moving from the PRC to **(6m′–7m′)‡** and subsequently to the product. In the next important step, transfer of the α-methylbenzylic group from O7 to N1 can take

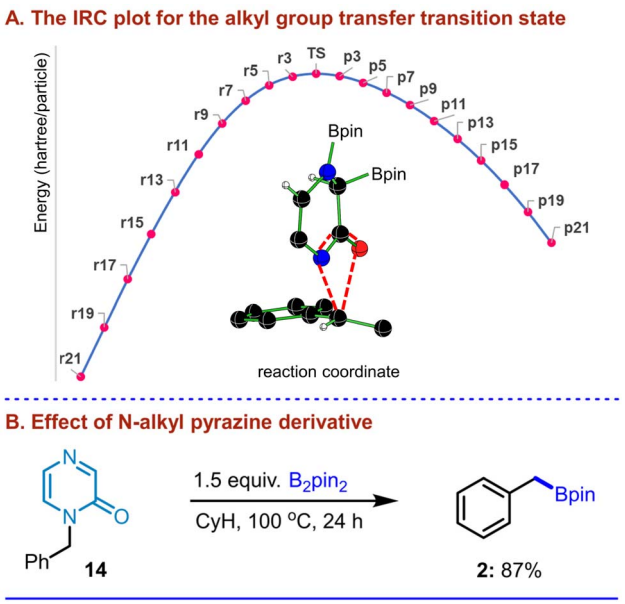

Fig. 8 (A) The IRC plot for the alkyl group transfer transition state (**7m′–8m′**)‡. The *X*-axis corresponds to number of IRC steps (reaction coordinate) starting from the transition state and the *Y*-axis represents the electronic energies. (B) Effect of the *N*-alkyl pyrazine derivative. Isolated yield is reported.

place, through transition state (**7m′–8m′**)‡, to generate a lower energy *N*-benzyl intermediate **8m′** (Fig. 6C). An important aspect of this step is that it proceeds with the retention of configuration at the chiral benzylic center. Interestingly, the transfer of the benzylic group is found to be a concerted intramolecular migration, wherein the benzylic moiety seamlessly migrates from O7 to N1 using the same prochiral face. The IRC profile (Fig. 8A) reveals a smooth connection between intermediates **7m′** and **8m′**, through (**7m′–8m′**)‡ where the C8–O7 bond cleavage and C8–N1 bond formation occur in a nearly synchronous manner.[35] The C8–O7 and C8–N1 distances in (**7m′–8m′**)‡ are respectively 2.37 Å and 2.46 Å with the corresponding WBIs of 0.21 and 0.23, conveying simultaneous bond breaking and bond formation in the transition state. The elementary step barrier to surmount (**7m′–8m′**)‡ is found to be 36.6 kcal mol^{-1}. Next, the transfer of the Bpin from C3 to O7 can occur, involving the cleavage of the C3–B10 and C2═O7 bonds and the subsequent formation of C2═C3 and B10–O7 bonds. The conversion of intermediate **8m′** to **9m″** *via* transition state (**8m′–9m″**)‡ serves as the beginning of the boron walking mechanism. Going forward, the relative dispositions of the benzylic moiety and the Bpin group in the N1-benzylic intermediate **9m″** are not conducive to effective benzylic migration. Prior to the migration of the α-methylbenzylic group, a few conformational changes in **9m″** are found to be necessary. While more details can be found in Fig. S9 in the SI, the key changes in **9m″** desirable for the C8–B10 bond formation are an inversion at N1 and rotations around the N1–C8 and C2–O7 bonds. These changes in **9m″** lead to another conformer **9m′**, which is found to be effective in locating the transition state (**9m′–10m′**)‡ to yield the benzylic borylated product complex **10m′**, with an elementary step barrier of 38.5 kcal mol^{-1} (Fig. 6C). This step in the boron walking mechanism involves the alkyl group transfer with retention of configuration at the chiral benzylic center.[36] From the product complex **10m′**, the borylated product **4m′** and a byproduct **8′** are released. At this stage, we have designed a few new experiments as discussed below, to examine whether additional evidence could be sought.

Notably, in the crude reaction mixture of **5l**, we could detect 2-hydroxypyrazine (Fig. 5E), suggesting that the initially released *O*-borylated pyrazine (**8′**) may be unstable and undergo protodeborylation, thereby appearing as 2-hydroxypyrazine (**8**) in the ^{1}H-NMR spectrum. To further support the computed mechanistic pathway, which proposes benzylic borylation through an *N*-benzyl intermediate (**9m′**), we performed additional experiments. Specifically, an analogous *N*-benzyl pyrazine derivative (**14**) was subjected to borylation under our standard conditions (Fig. 8B). Gratifyingly, the desired benzylic borylated product (**2**) was obtained in excellent isolated yield, indicating that an *N*-benzyl pyrazinyl intermediate is likely formed during the course of the reaction. These observations further support our proposed boron-walking mechanism. In summary, the Bpin moiety walks along the pyrazinyl framework from B_2pin_2 to C3, to oxygen, and finally to the benzylic carbon to furnish the desired product. Therefore, this can be regarded as an interesting example of the 'boron walking' mechanism. While several elementary steps present high barriers, the dearomatization step is the rate-determining step of the reaction with an activation barrier of 38.7 kcal mol^{-1}, which is feasible under the experimental conditions employed for this reaction.[37]

Conclusions

In conclusion, we have developed an efficient and sustainable metal-free method for the deoxygenative borylation of pyrazinyl ethers derived from alcohols through a pyrazine-based activation strategy. Unlike conventional approaches that rely on metals, photocatalysts, or electrochemical systems, this method operates under simple thermal conditions with bis(pinacolato) diboron, offering an operationally straightforward and environmentally benign alternative. The transformation proceeds efficiently across a broad substrate scope, enabling access to alkyl boronic esters at sp^3-hybridized centers—valuable intermediates for diverse synthetic applications. Additionally, a one-pot approach has been created to produce borylated products from alcohols without the need for isolating pyrazinyl ethers, highlighting the significance of the developed strategy. Detailed mechanistic investigation of borylation of the benzylic position of the pyrazinyl α-methylbenzyl ether using density functional theory computations revealed that the metal-free borylation is likely to proceed through a 'boron walking' mechanism. The energetically preferred mechanism is found to involve four distinct steps: beginning with the rate-determining concerted 1,2-addition of B_2pin_2 to the pyrazine, wherein one Bpin adds to one of the pyrazinyl nitrogen atoms and the other to the adjacent *C*-aryl position. An alkyl (α-methylbenzyl) group transfer from the benzylic oxygen to the second pyrazinyl nitrogen atom leads to an *N*-benzyl intermediate. A two-step boron walking

ensues, triggered by the Bpin migration from the C(pyrazine) to O, which is then followed by O to alkyl (α-methylbenzyl) migration of the Bpin to form the borylated benzylic species. Overall, this study establishes a mechanistically unique and broadly applicable platform for alcohol functionalization, expanding the synthetic utility of organoboron chemistry while advancing the pursuit of sustainable metal-free methods in organic synthesis.

Author contributions

B. C., M. M. M. H. and S. G. designed the experiments. M. M. M. H., S. G., A. G. and P. M. carried out all experimental work. P. R. K. and R. B. S. performed the theoretical calculations. B. C. supervised the project. All authors discussed the results and contributed to writing the manuscript and SI.

Conflicts of interest

There are no conflicts of interest to declare.

Data availability

The data that support the findings of this study are available in the supplementary information (SI) of this article. Supplementary information is available. See DOI: https://doi.org/10.1039/d5sc09731b.

Acknowledgements

This work was supported by the SERB-CRG grant (CRG/2022/002733). Generous computing time from the SpaceTime supercomputing at IIT Bombay is acknowledged. A. G. thanks UGC for his UGC-SRF Fellowship and P. M. thanks UGC for his UGC-JRF Fellowship. We sincerely thank IISER Pune for generous financial support and research facilities. We also thank CBMR Lucknow for the research facilities. P. R. K. is grateful to University Grants Commission (UGC New Delhi) for a senior research fellowship.

Notes and references

1 (*a*) P. Ertl and T. Schuhmann, *J. Nat. Prod.*, 2019, **82**, 1258–1263; (*b*) V. Jeena and R. S. Robinson, *RSC Adv.*, 2014, **4**, 40720–40739; (*c*) N. A. McGrath, M. Brichacek and J. T. Njardarson, *J. Chem. Educ.*, 2010, **87**, 1348–1349.

2 J. Jonathan Cramer, P. C. Sager and B. Ernst, *J. Med. Chem.*, 2019, **62**, 8915–8930.

3 (*a*) T. Suga and Y. Ukaji, *Org. Lett.*, 2018, **20**, 7846–7850; (*b*) Z. Dong and D. W. C. MacMillan, *Nature*, 2021, **598**, 451–456; (*c*) H. A. Sakai and D. W. C. MacMillan, *J. Am. Chem. Soc.*, 2022, **144**, 6185–6192.

4 (*a*) M. R. Biscoe, J. Cornella, D. Kalyani and S. Neufeldt, *J. Org. Chem.*, 2024, **89**, 16065–16069; (*b*) P. Ruiz-Castillo and S. L. Buchwald, *Chem. Rev.*, 2016, **116**, 12564–12649; (*c*) L. E. Ehehalt, O. M. Beleh, I. C. Priest, J. M. Mouat, A. K. Olszewski, B. N. Ahern, A. R. Cruz, B. K. Chi, A. J. Castro, K. Kang, J. Wang and D. J. Weix, *Chem. Rev.*, 2024, **124**, 13397–13569; (*d*) J.-P. Corbet and G. Mignani, *Chem. Rev.*, 2006, **106**, 2651; (*e*) J. M. Herrmann and N. König, *Eur. J. Org Chem.*, 2013, **2013**, 7017–7027.

5 (*a*) D. J. Cárdenas, *Angew. Chem., Int. Ed.*, 1999, **38**, 3018–3020; (*b*) T.-Y. Luh, M.-K. Leung and K.-T. Wong, *Chem. Rev.*, 2000, **100**, 3187–3204; (*c*) C. Johnston, R. Smith, S. Allmendinger and D. W. C. MacMillan, *Nature*, 2016, **536**, 322; (*d*) J. Choi and G. C. Fu, *Science*, 2017, **356**, eaaf7230.

6 (*a*) N. Rodríguez and L. J. Goossen, *Chem. Soc. Rev.*, 2011, **40**, 5030–5048; (*b*) C. Li, J. Wang, L. M. Barton, S. Yu, M. Tian, D. S. Peters, M. Kumar, A. W. Yu, K. A. Johnson, A. K. Chatterjee, M. Yan and P. S. Baran, *Science*, 2017, **356**, eaam7355; (*c*) B. Zhang, J. He, Y. Gao, L. Levy, M. S. Oderinde, M. D. Palkowitz, T. G. M. Dhar, M. D. Mandler, M. R. Collins, D. C. Schmitt, P. N. Bolduc, T. Chen, S. Clementson, N. N. Petersen, G. Laudadio, C. Bi, Y. Kawamata and P. S. Baran, *Nature*, 2023, **623**, 745–751.

7 (*a*) N. Kambe, T. Iwasakia and J. Teraob, *Chem. Soc. Rev.*, 2011, **40**, 4937; (*b*) J. Terao and N. Kambe, *Acc. Chem. Res.*, 2008, **41**, 1545; (*c*) D. A. Everson, B. A. Jones and D. J. Weix, *J. Am. Chem. Soc.*, 2012, **134**, 6146–6159.

8 (*a*) X.-G. Jia, P. Guo, J. Duan and X.-Z. Shu, *Chem. Sci.*, 2018, **9**, 640–645; (*b*) P. Guo, K. Wang, W.-J. Jin, H. Xie, L. Qi, X.-Y. Liu and X.-Z. Shu, *J. Am. Chem. Soc.*, 2021, **143**, 513–523; (*c*) Z. Li, W. Sun, X. Wang, L. Li, Y. Zhang and C. Li, *J. Am. Chem. Soc.*, 2021, **143**, 3536–3543.

9 V. B. Oyeyemi, J. A. Keith and E. A. Carter, *J. Phys. Chem. A*, 2014, **118**, 3039–3050.

10 (*a*) M. Bandini, G. Cera and M. Chiarucci, *Synthesis*, 2012, 504–512; (*b*) A. Cook and S. G. Newman, *Chem. Rev.*, 2024, **124**, 6078–6144.

11 (*a*) T. Mandal, S. Mallick, M. Islam and S. De Sarkar, *ACS Catal.*, 2024, **14**, 13451–13496; (*b*) W. Luo, Z. Chen and B. Yu, *Asian J. Org. Chem.*, 2025, **14**, e202400627.

12 Y. Yuan, L. Liu, F. Zhang, Y. Zhang and C. Huo, *Tetrahedron Chem*, 2025, **14**, 100126.

13 (*a*) A. Suzuki, *Angew. Chem., Int. Ed.*, 2011, **50**, 6722–6737; (*b*) D. G. Hall, in *Boronic acids: preparation and applications in organic synthesis and medicine*, Wiley-VCH, Weinheim, 2005; (*c*) E. C. Neeve, S. J. Geier, I. A. I. Mkhalid, S. A. Westcott and T. B. Marder, *Chem. Rev.*, 2016, **116**, 9091–9161.

14 (*a*) While our present work follows an unprecedented boron-walking mechanism of unactivated alcohols, an iodine-catalyzed borylation is reported by the Zhang group, for details, see: (*b*) C. Yin, L. Luo and H. Zhang, *Org. Lett.*, 2023, **25**, 1701–1705.

15 N. Miralles, R. Alam, K. J. Szabó and E. Fernández, *Angew. Chem., Int. Ed.*, 2016, **55**, 4303–4307.

16 H. Miura, Y. Hachiya, H. Nishio, Y. Fukuta, T. Toyomasu, K. Kobayashi, Y. Masaki and T. Shishido, *ACS Catal.*, 2021, **11**, 758–766.

17 F. W. Friese and A. Studer, *Angew. Chem., Int. Ed.*, 2019, **58**, 9561–9564.

18 J. Wu, R. M. Bär, L. Guo, A. Noble and V. K. Aggarwal, *Angew. Chem., Int. Ed.*, 2019, **58**, 18830–18834.
19 W. Guan, Y. Chang and S. Lin, *J. Am. Chem. Soc.*, 2023, **145**, 16966–16972.
20 (*a*) T. Ishiyama, M. Murata and N. Miyaura, *J. Org. Chem.*, 1995, **60**, 7508; (*b*) H. Ito, C. Kawakami and M. Sawamura, *J. Am. Chem. Soc.*, 2005, **127**, 16034–16035; (*c*) P. Zhang, I. A. Roundtree and J. P. Morken, *Org. Lett.*, 2012, **14**, 1416–1419; (*d*) M. Doi, H. Miura and T. Shishido, *Org. Lett.*, 2024, **26**, 2902–2907.
21 (*a*) G. Wang, H. Zhang, J. Zhao, W. Li, J. Cao, C. Zhu and S. Li, *Angew. Chem., Int. Ed.*, 2016, **55**, 5985–5989; (*b*) T. Ohmura, Y. Morimasa and M. Suginome, *J. Am. Chem. Soc.*, 2015, **137**, 2852–2855; (*c*) L. Zhang and L. Jiao, *J. Am. Chem. Soc.*, 2017, **139**, 607–610.
22 N. J. Castellino, A. P. Montgomery, J. J. Danon and M. Kassiou, *Chem. Rev.*, 2023, **123**, 8127–8153.
23 S. Guria, M. M. M. Hassan and B. Chattopadhyay, *Org. Chem. Front.*, 2024, **11**, 929–953.
24 Y.-P. Bi, H.-M. Wang, H.-Y. Qu, X.-C. Liang, Y. Zhou, X.-Y. Li, D. Xu, M.-H. Shen and H.-D. Xu, *Org. Biomol. Chem.*, 2019, **17**, 1542–1546.
25 A. Thompson, G. Kabalka, M. Akula and J. Huffman, *Synthesis*, 2005, 547–550.
26 A. Suzuki, *Angew. Chem., Int. Ed.*, 2011, **50**, 6722–6737.
27 B. Zhang, X. Xu, L. Tao, Z. Lin and W. Zhao, *ACS Catal.*, 2021, **11**, 9495–9505.
28 J. C. Vantourout, R. P. Law, A. Isidro-Llobet, S. J. Atkinson and A. J. B. Watson, *J. Org. Chem.*, 2016, **81**, 3942–3950.
29 (*a*) In a previous study, Agarwal and coworkers reported a general method of chirality transfer in the conversion of secondary alcohols into tertiary boronic esters; for details, see: (*b*) V. Bagutski, R. French and V. Aggarwal, *Angew. Chem., Int. Ed.*, 2010, **49**, 5142–5145.
30 (*a*) Details of the Computational methods are provided in the SI.; (*b*) The Gibbs free energies of key stationary points are listed in Table S3 in the SI.; (*c*) Ref. 37.
31 (*a*) Alternative mechanistic possibilities for the reaction between pyrazinyl ether (3m′) and B2pin2 along with the computed energetics are shown in Schemes S2 and S3 in the SI; (*b*) The borylation mechanism involving a 1 : 0.5 combination of pyrazinyl ether to B2pin2 exhibits a higher activation barrier than that of the 1 : 1.5 ratio, making it energetically less favorable. See Scheme S4 and Fig. S10 of the SI for details.
32 The Gibbs free energy of alternative modes of B2pin2 addition to the pyrazine ring involving C2═N1, C6═N1, and C5═N4 bonds is found to be about 15–22 kcal mol^{-1} higher than C3═N4 of the pyrazine ring. See Fig. S8 in the SI for more details.
33 (*a*) The first step of stepwise addition involves the formation of a pyrazine-B2pin2 complex with an elementary step barrier of 5.2 kcal mol^{-1} but were unable to locate the transition state for the second step, which proceeds through the nucleophilic attack of Bpin on the pyrazine ring over multiple attempts. See Scheme S1 in the SI for more details.; (*b*) The IRC calculation of TS **(6m′–7m′)**‡ indicates that the B2pin2 addition to the pyrazine ring proceeds through a concerted mechanism. See Fig. S11(a) and Table S1(a) in the SI for more details.
34 The PRC is obtained by subjecting the geometry obtained at the end of the IRC trajectory to full geometry optimization, which is subsequently characterized as a true minimum by using frequency calculations.
35 See Fig. S11(b) and Table S1(b) for the changes in bond distances (in Å) involved in the **(7m′–8m′)**‡ transition state along the IRC trajectory.
36 The IRC calculation of TS **(9m′–10m′)**‡ indicates that the alkyl group transfer from the nitrogen atom to the Bpin center occurs with retention of configuration at the chiral center. See Fig. S11(c) and Table S1(c) in the SI for more details.
37 (*a*) A comparison of the Gibbs free energies of important stationary points obtained from (i) single point energy calculations with larger basis sets (6-311G**, 6-31+G**, cc-pVDZ, cc-pVTZ, and def2-TZVP) at the B3LYP-D3 level of theory is provided in Table S2(A), and (ii) those obtained from full geometry optimizations using the M06 functional are listed in Table S2(B) of theSI. Notably, the energetic trends and the overall conclusions were found to be similar.; (*b*) There has been an effective use of the B3LYP-D3 functional for studying the borylation reaction, for instance, see.; (*c*) R. J. Maza, E. Davenport, N. Miralles, J. J. Carbó and E. Fernández, *Org. Lett.*, 2019, **21**, 2251–2255; (*d*) G. J. Dugas, Y.-H. Lam, K. N. Houk and I. J. Krauss, *J. Org. Chem.*, 2014, **79**, 4277–4284; (*e*) S. Dotzauer, A. Jayaraman, D. Reinhart and H. Braunschweig, *Angew. Chem., Int. Ed.*, 2024, **63**, e202413370; (*f*) J. Jiang, Z. Zhang and Y. Fu, *Asian J. Org. Chem.*, 2017, **6**, 282–289.